FUDMA Journal of Sciences (FJS)
ISSN online: 2616-1370
ISSN print: 2645 - 2944
Vol. 10 No. 8, April, 2026, pp 372 – 386
DOI: https://doi.org/10.33003/fjs-2026-1008-4903

Synthesis, Characterization, Multifunctional Bioactivity and Computation Study of 5-Fluorouracil-Thiamine HCl Mixed Ligands Complexes

***[1]Sheriff. O. Ayinla, [2]Abdullah. O. Rajee, [3,4]Louis. Hitler, [3,4]Francisca Bassey and [5]Hassan. K. Busari**

[1]Department of Chemical and Geological Sciences, Al-Hikmah University, Ilorin, Kwara State, Nigeria.
[2]Department of Chemistry, University of Ilorin, Ilorin, Kwara State, Nigeria.
[3]Department of Pure and Industrial Chemistry, University of Calabar, Calabar, Nigeria.
[4]Centre of Molecular Modelling and Simulation, University of Cross River State, Calabar, Nigeria.
[5]Department of Pure and Applied Chemistry, Osun State University, Osogbo, Osun State, Nigeria.

*Corresponding authors' email: sheriffayinla@alhikmah.edu.ng Phone No.: +2349067136512

ABSTRACT

This study explored the structural, spectroscopic and biological properties of Ni(II) and Zn(II) mixed-ligand complexes of 5-fluorouracil–thiamine HCl synthesized through one-pot synthetic method using integrated approaches including computational study. 5-fluorouracil acts as bidentate ligand through nitrogen and carbonyl oxygen atoms of the pyrimidine ring while the thiamine HCl acts as monodentate through nitrogen atom of its pyridinic ring. Geometry optimization demonstrated that the Ni(II) complex exhibits shorter and stronger metal–ligand bonds, particularly with nitrogen and oxygen donor atoms, reflecting enhanced covalent character and greater structural distortion compared to the Zn(II) complex, which showed relatively longer and more ionic interactions. The Ni(II) complex exhibited better antimicrobial and antioxidant properties compared to the Zn (II) complex and the 5-flourouracil ligand. The molecular docking studies indicated that the two complexes showed superior binding affinities against both bacterial (1KZN) and fungal (5TZ1) target proteins compared to standard drugs but Ni (II) complex exhibited excellent antibacterial activity with a Moldock score of −153.39 kcal/mol and strong hydrogen bonding interactions (Val 71, Thr 65, and Asn 46), outperforming the standard drug Ciprofloxacin, which showed a lower binding affinity (−117.39 kcal/mol) and fewer hydrogen bonds. Similarly, both complexes demonstrated remarkable antifungal activity, with Zn (II) complex showing particularly strong binding (−131.12 kcal/mol) and favorable interactions with key residues (Ile 471, Tyr 132, and Arg 381), surpassing the performance of the Fluconazole standard, which exhibited weaker interaction profiles.

Keywords: 5-Flourouracil, Bioactivity, Molecular Docking, Geometry Optimization

INTRODUCTION

Metal-based compounds have emerged as a major class of therapeutic agents because transition metals provide chemical capabilities that organic molecules alone cannot achieve. Experimental coordination studies of metal-based compounds consistently show that metal chelation enhances cellular uptake and radical scavenging capacity, establishing metal–ligand synergy as a fundamental principle in therapeutic design (Elgazar et al., 2025). Zinc (II) and nickel(II) ions occupy significant positions in bioinorganic chemistry because of their enzymatic and antimicrobial relevance. Zinc functions as a structural and catalytic component in numerous metalloenzymes responsible for gene expression and protein stabilization. Its redox-inert character allows biological participation without uncontrolled oxidative reactions. Nickel complexes, although less prevalent physiologically, exhibit strong antimicrobial behaviour and catalytic versatility. Coordination compounds containing Zn(II) and Ni(II) frequently display enhanced biological activity compared with free ligands, supporting their continued exploration in medicinal inorganic chemistry (Yadav et al, 2025). 5-Fluorouracil (5-FU) remains one of the most widely applied antimetabolite drugs in cancer therapy due to its ability to disrupt nucleotide biosynthesis. Structurally, 5-FU is a fluorinated pyrimidine analogue that inhibits thymidylate synthase and interferes with DNA and RNA processing, leading to suppression of rapidly dividing cells. Despite decades of clinical use, resistance to 5-FU continues to challenge oncological treatment. Tumor cells may alter metabolic activation pathways, enhance DNA repair mechanisms, or suppress apoptosis, reducing drug effectiveness. These limitations have motivated investigation into coordination strategies that modify 5-FU through metal binding to improve delivery, stability, and multifunctional biological scope (Gmeiner & Okechukwu, 2023). Thiamine hydrochloride (vitamin B1) adds important biochemical functionality to mixed-ligand coordination systems. Thiamine is an essential metabolic cofactor involved in carbohydrate metabolism and cellular energy production. Its physiological importance extends to protection against oxidative stress and maintenance of intracellular redox balance. The molecular structure of thiamine contains donor atoms capable of coordinating transition metals, enabling formation of stable complexes with biomedical relevance. Incorporating thiamine into coordination frameworks enhances solubility, antioxidant behavior, and metabolic compatibility, making it a valuable ligand in bioactive metal complexes (Hrubša et al., 2022). Modern drug development increasingly favors multifunctional systems capable of addressing multiple biological targets simultaneously. Mixed-ligand metal complexes represent an advanced design strategy in which pharmacologically distinct ligands cooperate within a single coordination environment to modulate electronic structure, lipophilicity, and biological selectivity. Integrating 5-fluorouracil and thiamine hydrochloride within Zn(II) and Ni(II) frameworks offers a rational platform for generating compounds that combine cytotoxic, antibacterial, antifungal, and antioxidant properties. Such multifunctional systems expand the therapeutic scope of individual components and highlight the role of coordination chemistry in next-generation biomedical innovation (Marinova & Blazheva, 2025). The study of mixed-ligand Zn(II) and Ni(II) complexes

derived from 5-fluorouracil and thiamine hydrochloride therefore lies at the intersection of inorganic chemistry and therapeutic design. By combining established pharmacophores with biologically relevant metal ions, these systems provide a framework for investigating structure–activity relationships and multifunctional bioactivity. Continued exploration of such complexes will contribute to a deeper understanding of how coordination chemistry can enhance drug performance and supports the development of safer, more effective metal-based therapeutics (Omer, et al., 2024).

MATERIALS AND METHODS

Materials

The two ligands were purchased from Sigma-Aldrich, Germany. The metal salts were obtained from Chemistry Department, University of Ilorin. Both Ni(II) and the Zn (II) salts are products of BDH Chemical Ltd in Poole, England. All solvents and other reagents for the synthesis were used without further purification. The OptiMelt Automated Melting Point System was used to determine the melting points of the ligands and complexes. A FLASH WA 1112 Series by Thermo Finnigan Italy was used for the CHN analysis while a Shimadzu FTIR-8501 Spectrometer was used to record the FTIR spectra on KBr powder. The UV spectra were recorded in DMSO solution in the range 200 - 900nm using Shimadzu UV 1800 spectrophotometer.

Methods

Synthesis of the Metal Complexes

1mmol (0.130 g) of 5-flourouracil was dissolved in 10 ml distilled water and few drops of aqueous ammonia was added then stirred to dissolve. 20ml methanolic solution of nickel acetate tetrahydrate (1 mmol) was further added and stirred for two hours. 2mmol (0.675g) of thiamine HCl was added to the mixture and stirred at room for further 3 hours. The pH of the solution was adjusted to about 9 with addition of drops of aqueous ammonia and the filtrate kept for 94 days to obtain another greenish product which was washed with methanol-water (50%:50%) severally and air-dried. Compound **(2)** was obtained as white crystalline solid following similar method but using zinc acetate dehydrate.

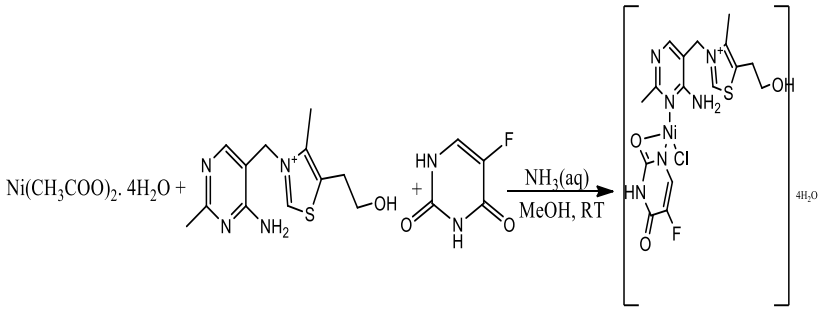

Figure 1: Reaction Scheme for Synthesis of $[Ni(fu)(thm)(Cl)].(H_2O)_4$

Yield: 58%, M.Wt. = 562.65g/mol, M.pt = 310°C, CHN: Found (Cal) % for $C_{16}H_{27}ClFN_6O_7SNi^+$; C, 35.49 (34.28); H, 5.88 (4.85); N, 14.63 (14.99). FTIR (KBr, cm^{-1}): 3501, 3441, 3339, 3235, 3109, 2970, 2778, 2362, 2037, 1659, 1614, 1560, 1481, 1381, 1282, 1232, 1159, 1045, 997, 943, 866, 775, 750, 679, 644, 596, 573, 503, 461.

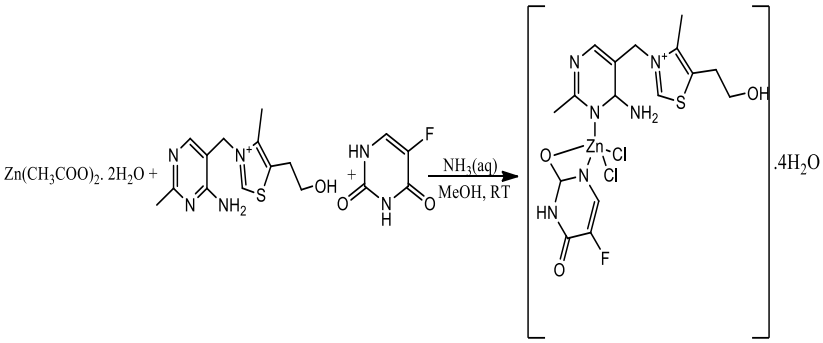

Figure 2: Reaction Scheme for Synthesis of $[Zn(fu)(thm)(Cl_2)].(H_2O)_4$

Yield: 45 %, M.Wt. = 604.8 g/mol, M.pt = 297 °C, CHN: Found (Cal) % for $C_{16}H_{27}Cl_2FN_6O_7SZn^+$; C, 32.38 (31.88); H, 3.76 (4.51); N, 12.67 (13.94). FTIR (KBr, cm^{-1}): 3418, 3333, 3234, 3088, 2930, 2446, 2361, 2093, 1643, 1616, 1535, 1500, 1437, 1350, 1282, 1236, 1171, 1072, 993, 928, 854, 787, 679, 648, 586, 488, 453.

Antibacterial and Antifungal Assays

The antibacterial activity of the metal complexes was assessed using the agar diffusion method against three clinical laboratory strains of Gram-positive bacteria: *Staphylococcus aureus, Pseudomonas aeruginosa, and Escherichia coli*. The antifungal activity of the metal complexes were evaluated against *Candida albicans, Aspergillus niger, and Aspergillus flavus* using the same methodology with modifications. The sterile media was poured and allowed to solidify in sterilized petri dishes for about 20 minutes. The media was inoculated with 100µL of microorganism. Each sample was placed on a bore of disc of diameter 5mm. The petri dishes were inoculated at 37 °C for 24 hours and 30 °C for 48 hours respectively for the bacteria and the fungal strains after which the zone of inhibition was measured in millimeter. Duplicates of the inhibitory activity were carried out and average determined in millimeter. The negative control was a medium with DMF as the solvent, while the positive controls were

media with ciprofloxacin and fluconazole for antibacterial and antifungal activities respectively.

Antioxidant Potential Determination

The Blois method for the DPPH (2, 2-diphenyl-1-picrylhydrazyl)-free radical scavenging assay was adapted (Yusuff *et al*., 2019) with modifications. Two hundred (200) cm^3 of absolute ethanol was used to dissolve 2 mg of DPPH to make a 0.02540 mM stock solution. Four further concentrations 0.01270, 0.00635, 0.00313 and 0.00156 mM were obtained using serial dilution of the stock solution. Using a UV spectrophotometer at 517 nm, the absorbance of each solution was measured twice. In order to calculate the molar absorptivity of DPPH from the slope, absorbance was plotted versus concentrations. Each sample and ligand were generated in five further concentrations: 0.50000 mg/ml, 0.25000 mg/ml, 0.12500 mg/ml, 0.06250 mg/ml, and 0.03125 mg/ml. Each sample, (2 ml), was shaken vigorously with (2 ml) 0.0254 mM DPPH solution for 2 minutes in various test tubes. Each test tube was incubated in the dark for 45 minutes. The absorbance of each test tube solution was read at 517 nm. The absorbance of the blank and ascorbic acid were also recorded. Each compound's percentage inhibitory effect was calculated as:

% scavenging effect = $\frac{A_C - A_S}{A_C}$ x 100%.

The IC_{50} value for the compounds and ligand, or the sample concentration required to inhibit 50% of the DPPH free radical, was calculated using IC_{50} calculator on https://www.aatbio.com/tools/ic50 - calculator.

RESULTS AND DISCUSSION

Physicochemical Properties of Mixed Ligand Metal Complexes of 5-Flourouracil and Thiamine HCl

The melting point of the compounds (1) [Ni(fu)(thm)Cl].4(H_2O) and (2) [Zn(fu)(thm)Cl_2].4(H_2O) are higher than ligands' melting points, thiamine HCl and 5-fluorouracil. This shows that a strong bond is formed between the central metal ions and the ligands, 5-flouroracil and thiamine HCl. Compound (1) [Ni(fu)(thm)Cl].4(H_2O) is an hydrated greenish powdered compound; characteristic colour of transition metal complexes while Compound (2) [Zn(fu)(thm)Cl_2].4(H_2O) is also an hydrated white coloured crystalline compound since zinc (II) ion in its compounds has completely filled d-orbital sub-shell which does not permit transition between the orbitals sub-shells (Tyagi et al., 2020). The percentage yield of the compounds (1) and (2) are 58% and 45% respectively. Analysis of the compound (1) [Ni(fu)(thm)Cl].4H_2O using elemental CHN and compound (2) [Zn(fu)(thm)Cl_2].4H_2O shows that the estimated elemental composition percentage values (Table 1) for the proposed structures are well-aligned with the experimental values, indicating that the metal ions and the ligands, 5-fluorouracil and thiamine HCl, coordinated to form the compounds (Althubeiti, 2025).

Table 1: Physicochemical Properties of Mixed Ligand Metal Complexes of 5-Flourouracil and Thiamine HCl

Ligand /Complex	Appearance/Solid State	Yield (%)	M. Wt (g/mol)	M.pt (°C)	Elemental Analysis: % found (% calc)		
					C	H	N
(1) [Ni(fu)(thm)Cl].4H_2O	Green Powder	58	562.65	310	35.49 (34.15)	5.88 (5.20)	14.63 (14.94)
(2) [Zn(fu)(thm)Cl_2].4H_2O	White Crystalline Solid	45	604.80	297	32.38 (31.77)	4.83 (5.88)	13.90 (14.63)

FTIR Spectra of Mixed Ligand Metal Complexes of 5-Flourouracil and Thiamine HCl

The selected IR data for the ligands, 5-flourouracil, thiamine HCl and the metal complexes, (1) [Ni(fu)(thm)Cl].4H_2O and (2) [Zn(fu)(thm)Cl_2].4H_2O are shown on Table 2 below.

Table 2: Selected FTIR Data for 5-Flourouracil, Thiamine HCl and Mixed Ligand Metal Complexes of 5-Flourouracil – Thiamine HCl

Ligand/Complex	N-H stretch/bend	C=O	C-F	-OH	-C=N	=C-S	M-L
fu	3069 1502	1725 1667	1246	-	-	-	-
thm	-	-		3493	1666	1170	-
(1) [Ni(fu)(thm)Cl].4H_2O	3109 1580	-1659	1233	3501 3441	1614	1159	644 679
(2) [Zn(fu)(thm)Cl_2].4H_2O	3088 1535	1643	1233	3418	1616	1171	648 679

A shift to lower wavenumber was observed for the -N-H stretch band of the ligand 5-flourouracil at 3069cm^{-1} to 3109 cm^{-1} in the IR spectra of compound **(1) [Ni(fu)(thm)Cl].4(H_2O),** indicating the participation of a nitrogen atom on the pyrimidine ring of the 5-fluorouracil in the formation of compound **(1) [Ni(fu)(thm)Cl].4(H_2O)**. Broad band at wavenumber range between 3500 cm^{-1} to 3100 cm^{-1} (Table 2) suggesting presence of water molecules in the structure of compound **(1) [Ni(fu)(thm)Cl].4(H_2O),** (Pasieczna-Patkowska *et al*., 2025) also reported presence of water molecules in the structure of metal complexes as a result of broad band at about 3400 cm^{-1} wavenumber**.** The band at 1725 cm^{-1} assigned to one of the carbonyl groups on the IR spectrum of ligand, 5-flourouracil was observed to have disappear in the IR spectrum of compound **(1) [Ni(fu)(thm)Cl].4(H_2O)** suggesting coordination through the carbonyl group (Figure 3). A significant shift in the –C-F band from 1246 cm^{-1} to 1233 cm^{-1} is an indication of 5-flourouracil participation in the formation of the complex (**1) [Ni(fu)(thm)Cl].4(H_2O)** (Silva *et al*., 2018). The aromatic –C=N band assignment, 1666 cm^{-1} in the IR spectrum of thiamine HCl undergo a significant shift to 1614 cm^{-1} (Figure 3) suggesting coordination through nitrogen atom of pyrimidine ring of the thiamine HCl. The New bands at 644 cm^{-1} and 679 cm^{-1} in the fingerprint region also suggest formation of new compound (Figure 3). Similar assignment was observed in the IR spectrum of compound **(2) [Zn(fu)(thm)Cl_2].4(H_2O)** with a broad band shift from 3069 to 3088 cm^{-1} (Figure 4) suggesting presence of uncoordinated water molecules and participation of nitrogen atom of

aromatic ring of the 5-flourouracil. Disappearance of the band at 1725 cm^{-1} assigned to the carbonyl group on the spectrum of compound **(2)** suggests coordination to the zinc metal through oxygen of the carbony l group of 5-flourouracil (AL-Nama *et al*., 2025). A significant shift of the wavenumber 1666 cm^{-1} of the N-atom of thiamine HCl pyrimidine ring to 1616 cm^{-1} indicate monodentate mode coordination of the secondary ligand, thiamine HCl (Carballo Rial et al., 2012).

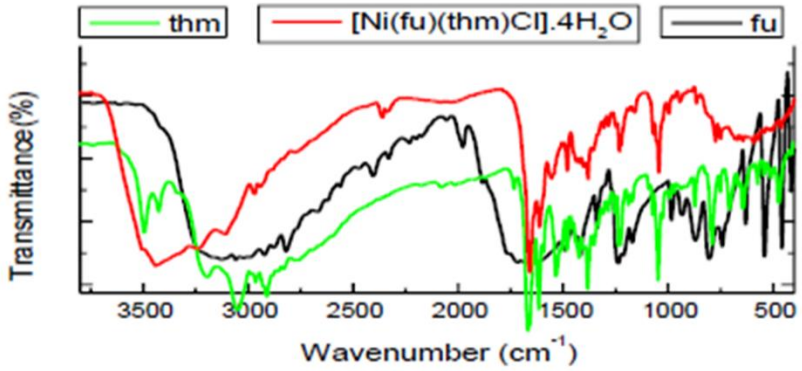

Figure 3: FTIR Spectrum of Nickel Complex of 5-Fluorouracil-Thiamine HCl

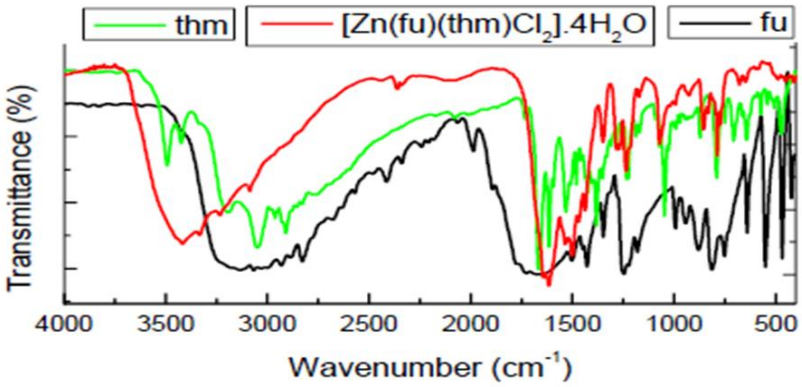

Figure 4: FTIR Spectrum of Zinc Metal Complex of 5-Fluorouracil-Thiamine HCl

Electronic Spectra of Mixed Ligand Metal Complexes of 5-Flourouracil and Thiamine HCl

The UV-Vis spectra data and the respective assignments for the metal complexes of mixed ligand 5-flourouracil- thiamine HCl and that of the ligands are shown on Table 3.

Table 3: Selected UV-Vis Spectra Data and Proposed Geometry of Mixed Ligand Metal Complexes of 5-Flourouracil - Thiamine HCl

Ligand/Complex	Medium	Wavelength(nm)	Assignment
Fu	DMF	273	$\pi \rightarrow \pi^*$
		280	$n \rightarrow \sigma^*$
		331	$n \rightarrow \pi^*$
Thm	DMF	268	$\pi \rightarrow \pi^*$
			$n \rightarrow \pi^*$
(1) [Ni(fu)(thm)Cl].4(H_2O)	DMF	283	$\pi \rightarrow \pi^*$
		340	$n \rightarrow \pi^*$
		377	LMCT
(2) [Zn(fu)(thm)Cl_2].4(H_2O)	DMF	273	$\pi \rightarrow \pi^*$
		313	LMCT

The selected data for the UV-Vis spectral of the ligands 5-flourouracil, thiamine HCl and that of the metal complexes of the ligands are shown on Table 3. Compound (1) [Ni(fu)(thm)Cl].4(H_2O) also has intraligand transitions at 283 nm and 340 nm; the weak absorption band observed at 377 nm can be assigned to ligand – metal charge transfer (LMCT) transition, suggesting formation of the complex as square planar in geometry; similar observation was reported for square planar complexes with three intense peaks in the region ranges between 256 – 402 nm, (Hemingway, 2020). Compound (2) [Zn(fu)(thm)Cl_2].4(H_2O) shows only two absorption bands at 273 and 313 nm with proposed structure as trigonal bipyramid which was reported as unusual geometry for zinc (II) complexes (Liu, 2022; She *et al*, 2020). With characteristic full d- valence electrons in Zn (II) ion, a stable 18-electron complex can be obtained through 4-coordination number with its ligand therefore a 5-coordination number of Zn (II) ion with its ligand will render the complex unstable and unusual.

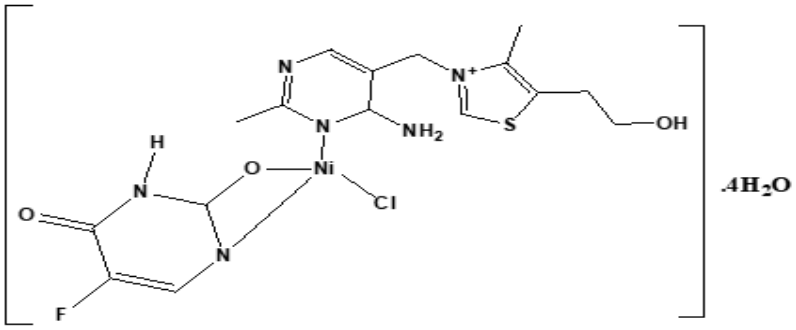

Figure 5: Proposed structure of Compound (1), [Ni(fu)(thm)Cl].4H_2O

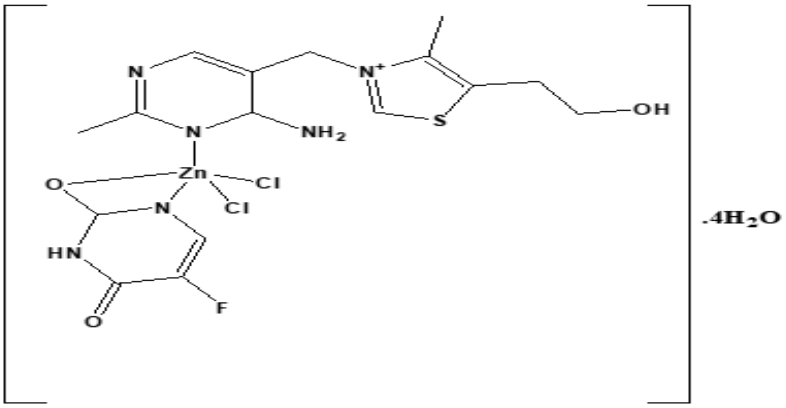

Figure 6: Proposed Structure of Compound (2), [Zn(fu)(thm)Cl_2].4H_2O

Antimicrobial Studies of Mixed Ligand Metal Complexes of 5-Flourouracil and Thiamine HCl

Compound **(1)** showed the strongest activity against *Pseudomonas aeruginosa* compared to the ligand 5-flourouracil and the ciprofloxacin positive reference standard (Figure 7). Compound **(2)** also showed higher inhibition against *Pseudomonas aeruginosa* strain. The two compounds **(1)** and **(2)** exhibited better antibacterial activity against *Staphylococcus aerues* compared to the positive reference and the ligand 5-flourouracil. Presence of electron withdrawing chlorine atoms in the two compounds **(1)** and **(2)** in addition to the chelating influence of the metal ions on the ligands may explain the improved antibacterial activity of the compounds (Ahmed et al., 2023).

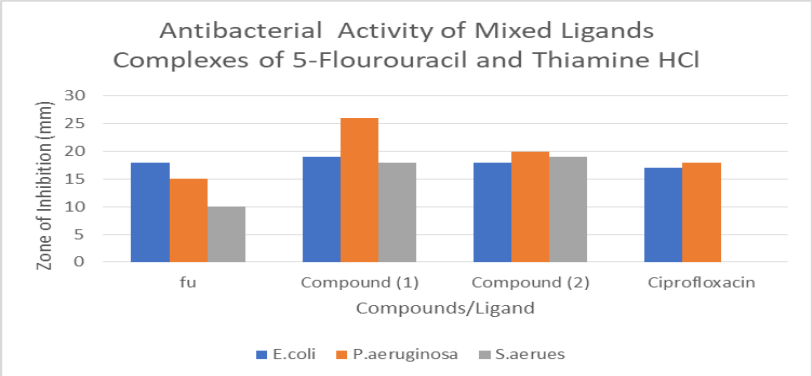

Figure 7: Antibacterial Activity of Mixed Ligand Metal Complexes of 5-Flourouracil - Thiamine HCl

Compound (1) [Ni(fu)(thm)Cl].4H_2O competes favourably in terms of antifungal effect with the ligand 5-flourouracil and fluconazole against the three fungi strains *Candida albicans*, *Aspergillus niger and Aspergillus flavus*. Also the fluconazole has not shown any prominent zone area of inhibition against *Aspergillus flavus*. The Compound (2) [Zn(fu)(thm)Cl_2].4(H_2O) also shows improved antifungal activity against the fungus strain *Aspergillus niger* though lower than zone of inhibition for fluconazole, similar observation was reported by Jamil et al, (2025) for metal complexes. No prominent zone of inhibition was observed for the compound (2) against *Candida albicans* (Figure 8).

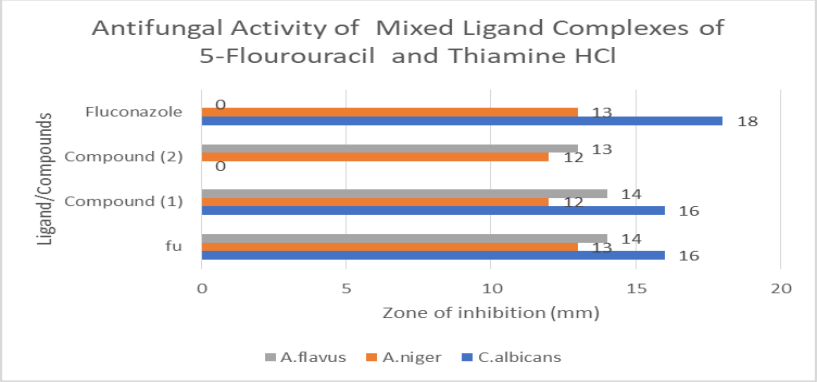

Figure 8: Antifungal Activity of Mixed Ligand Metal Complexes of 5-Flourouracil - Thiamine HCl

Antioxidant Study of Mixed Ligand Metal Complexes of 5-Flourouracil - Thiamine HCl

Compound (1) Ni(fu)(thm)Cl].4(H_2O) shows a good antioxidant activity compare to compound (1) and the ligand, 5-flourouracil but compound (2) and the ligand 5-flourouracil both compete favourably in terms of their DPPH radical percentage inhibition (Figure 9). The IC_{50}–value of compound (1) [Ni(fu)(thm)Cl].4(H_2O) is of lower size (Figure 10) indicating that the compound is a better antioxidant agent compared to the ligand 5-flourouracil and compound (2) [Zn(fu)(thm)Cl_2].4(H_2O) (Figure 10). The extensive aromatic ring and uncoordinated hydroxyl group on the secondary ligand, thiamine HCl coupled with chelation of metal centres with the ligands may explain the improved antioxidant capacity of compound (1) [Ni(fu)(thm)Cl].4(H_2O) compared to 5-flourouracil (Melo-Betances et al, 2025).

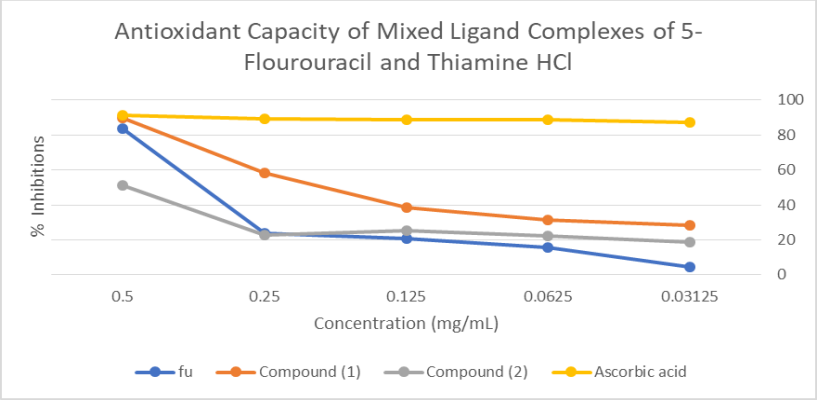

Figure 9: % Inhibition of DPPH Radical by Mixed 5-Flourouracil and Thiamine HCl Metal Complexes

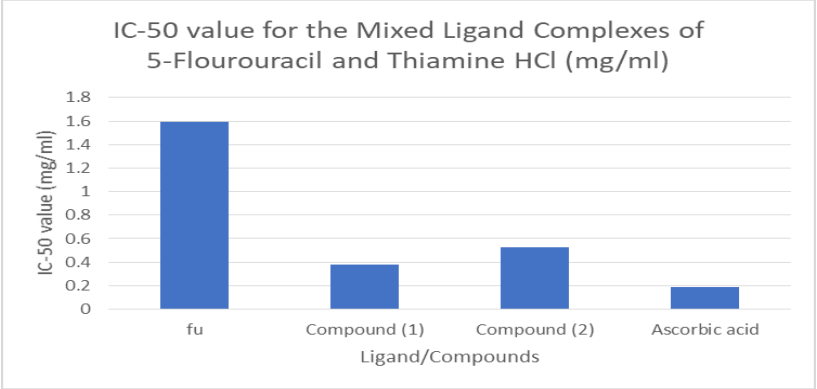

Figure 10: IC_{50} - Value of DPPH Radical Inhibition by Mixed 5-Flourouracil and Thiamine HCl Metal Complexes

Computational Study

DFT Calculations

All quantum chemical calculations were carried out using Density Functional Theory (DFT) as implemented in standard computational chemistry software packages. The geometries of the studied Ni(II) and Zn(II) mixed-ligand complexes were fully optimized without symmetry constraints using the hybrid functional B3LYP augmented with Grimme's dispersion correction (B3LYP-D3), which accounts for long-range dispersion interactions critical for accurately describing noncovalent effects **(**Koller et al,2020). The Def2-SVP basis set was employed for all atoms, providing a balanced description of valence and polarization functions suitable for transition metal complexes **(**Hellweg & Rappoport., 2015). Computations of frequencies were done at the same theory level to ensure that the optimized structures are actual minima

of the potential energy surface as shown by the non-existence of imaginary frequencies.

Follow up calculations, such as, Frontier Molecular Orbital (FMO), Natural Bond Orbital (NBO), Molecular Electrostatic Potential (MESP), Quantum Theory of Atoms in Molecules (QTAIM) and Non-Covalent Interaction (NCI) calculations were conducted on the optimized geometries. The NBO analysis was employed to assess the interactions between donors and acceptors and charge delocalization and topological parameters (electron density and Laplacian at bond critical points) were calculated using the QTAIM analysis. To visualize the charge distribution and places of reactive sites, images of MESP surfaces were created and NCI analysis was carried out with reduced density gradient (RDG) isosurfaces to describe weak interactions involving molecules. To perform biological assessment, Molegro docking software **(**Bitencourt-Ferreira & de Azevedo Jr, 2019) was used to test the binding of the complexes with their molecular targets on the selected bacterial (PDB ID: 1KZN) and fungal (PDB ID: 5TZ1) proteins **(**Berman et al., 2000). The potential therapeutic value of the complexes was evaluated by the binding affinities, hydrogen bonding interactions and steric contacts with the standard pharmaceutical drugs. A combination of the above-mentioned computational methodologies gives a robust and multifaceted overview of the structural, electronic and biological aspects of the complexes that are studied.

Table 4: Optimized bond lengths (Å) of Ni (II) and Zn (II) Mixed-Ligand Complexes Showing Metal–Ligand Coordination and Key Intraligand Structural Parameters

Compound	M-Cl	M-O	M-N	C-F	C-S	O-H	C=O	C-O
Ni Ligand	2.258	1.860	1.840	1.346	1.784	0.965	1.222	1.394
Zn Ligand	2.229	1.863	2.051	1.375	1.718	0.965	1.212	1.370

Geometry Optimization

These geometry optimization outcomes of the Ni(II) and Zn(II) mixed-ligand complexes of the 5- fluorouracil - thiamine HCl in Table 4 indicate the slight but significant difference in the coordination behavior and distortion of the structure. The lengths of the metal-chloride bond are a little bit shorter in the Zn complex (2.229 A) than in the Ni complex (2.258 Å), indicating a stronger or more electrostatic association in the Zn system (Inah et al., 2025). Conversely, the metal-oxygen bond distances are nearly identical in both complexes (Ni, O: 1.860 Å; Zn, O: 1.863 Å), and the contributions of the oxygen donor atoms to stabilize both metal centers are similar. Å greater difference in the length of metal-nitrogen bonds is seen in that the Ni -N (1.840 Å) bond is shorter than the Zn -N (2.051 Å) bond and suggests that Ni (II) has a stronger and more covalent interaction with the nitrogen donor sites, whereas, the Zn (II) has a weaker interaction with the nitrogen. The differences in the internal ligand-bond parameters also represent another effect of metal coordination. The B and C bond between C and F are a little longer in the Zn complex (1.375 Å) compared to that of Ni (1.346 Å), indicating that there is slight redistribution of electrons. In the Zn complex, the CS bond is shorter (1.718 Å) than in the Ni complex (1.784 Å), meaning that the sulfur moiety in the complex is less perturbed in the Zn system. The length of the O-H bond is also the same (0.965 A) in both complexes, indicating that hydroxyl groups do not play a major role in the coordination. Nevertheless, the carbonyl (C=O)-length of the bonds and the C-O bonds are slightly extended in the Ni complex (1.222 Å and 1.394 Å, respectively) as compared to the Zn complex (1.212 Å and 1.370 Å) which indicates a higher interaction of the Ni (II) with the oxygen based functional groups as the ligand structure becomes more deformed as indicated in Figure 11. These findings suggest that the Ni (II) complex is more forceful. The Zn (II) complex, by contrast, exhibits comparatively weaker and more ionic interactions and retains a significant proportion of the geometry of the ligand.

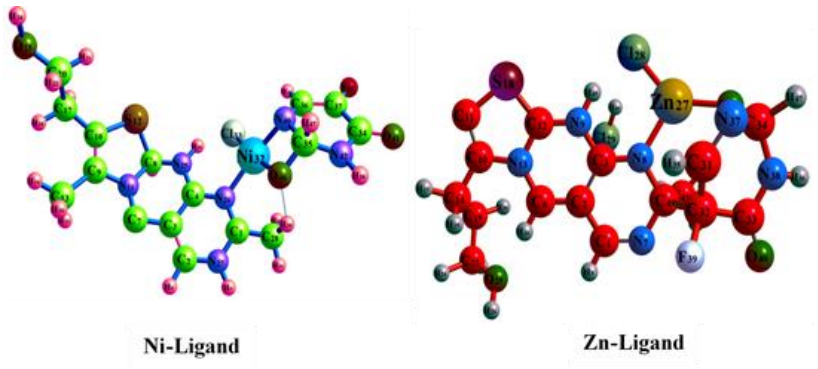

Figure 11: Optimized Molecular Structures of Ni(II) and Zn(II) Mixed-Ligand Complexes

Frontier Molecular Orbital (FMO) Analysis

The analysis of FMO alongside the HOMO-LUMO contour plots gives a good understanding of the electronic structure and reactivity difference between the Ni(II) and Zn(II) complexes of the mixed-ligand complexes. In the case of the Ni complex, HOMO energy (-4.191 eV) and LUMO energy (-3.517 eV) give very small value of the energy gap (0.674 eV) and this is also graphically supported by the FMO diagram as the electron density distribution between HOMO and LUMO is relatively continuous (Aihara, 1999). Figure 12 shows electron density is mostly delocalized through the ligand framework (especially across the heteroatoms (N, O, and S) and conjugated carbon), and is strongly π-characterized and capable of significant overlap with the Ni center. When excited to the LUMO, the electron density changes but is still highly dispersed throughout the backbone of both the ligand and the metal center, indicating an intramolecular charge transfer (ICT) mechanism, consuming both the metal center and ligand orbitals. This narrow band gap and large delocalization is associated with low global

hardness (η = 0.337 eV) and extremely large softness (22.035 eV), meaning that the Ni complex is chemically more reactive, more polarizable, and more susceptible to taking part in electron transfer reactions. These are usually linked to increased biological activity since the complex is able to interact easily with biomolecular targets. Conversely, the Zn complex has a lower HOMO energy (-5.930 eV) and a greater LUMO energy (-3.052 eV), resulting in a greatly larger energy gap (g = 2.878 eV). This difference is readily apparent in the FMO images, in which the HOMO is more localized, and largely confined to individual fragments of the ligand (in particular, around the donor atoms), and the delocalization to the Zn center is less effective. Electron density in LUMO has been moved to other parts of the ligand, although the whole distribution is more fragmented than in the Ni complex. This shows that there is a less efficient intramolecular charge transfer pathway. The increased band gap indicates increased hardness (η = 1.439 eV) and reduced softness (7.007 eV) meaning that the Zn complex is less susceptible to chemical attacks, reactive, and polarizable. Also, it is more electronegative (χ = 4.491 eV) which indicates more potential to attract electrons, yet the lower softness also reduces its reactive capacity.

Table 5 together with a visual FMO analysis of the results show that the Ni complex has a small HOMO-LUMO gap due to a highly delocalized electronic system that is capable of charge transfer and increases reactivity. Conversely, the Zn complex has a more delocalized structure with larger energy gap and less reactive, which makes it more kinetically stable. The latter differences in electronics are key to the variation in their chemical activity and possible bioactivity, as the Ni complex is probably more interactive at the molecular level, where the Zn complex has more selective and regulated interactions.

Table 5: Frontier Molecular Orbital (FMO) Parameters Including HOMO, LUMO, Energy Gap (ΔE), Global Hardness (η), Electronegativity (χ), and Softness (S) of Ni and Zn Complexes

Compound	HOMO-eV	LUMO-eV	ΔE-eV	η-eV	□-eV	□-eV
Ni Ligand	-4.191	-3.517	0.674	0.337	3.854	22.035
Zn Ligand	-5.930	-3.052	2.878	1.439	4.491	7.007

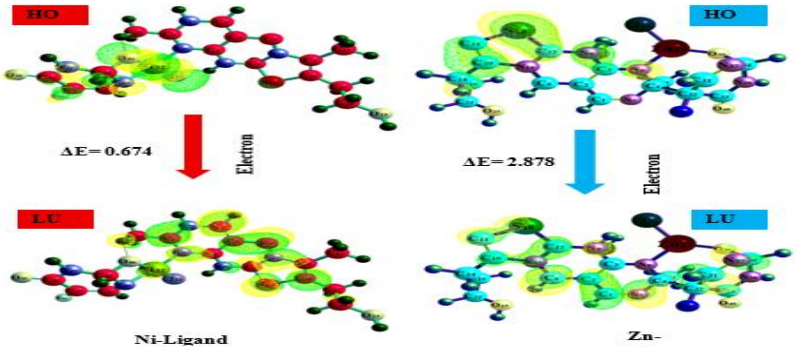

Figure 12: HOMO and LUMO Orbital Distributions of Ni(II) and Zn(II) Complex Showing Electron Density Delocalization And Charge Transfer

Fourier-Transform Infra-Red (FTIR) Analysis

FTIR spectral data of the mixed-ligand complexes of Ni(II) and Zn(II) have significant evidence of coordination modes and functional group participation of bonding. According to a comparative evaluation of **Table 6**, similarities and discrete changes are revealed, which depicts the dissimilarity in metal-ligands interactions **(**Glendening et al., 2019). The O–H symmetric stretching vibrations appear at 3831.30 cm^{-1} for the Ni complex and 3837.23 cm^{-1} for the Zn complex, with only a slight shift, indicating that hydroxyl groups are largely non-coordinating or only weakly involved in hydrogen bonding rather than direct metal coordination. Similarly, the N–H symmetric stretching bands occur in a very close range (Ni: 3599.47, 3595.63 cm^{-1}; Zn: 3597.52 cm^{-1}), suggesting that amine groups are not significantly perturbed, although minor shifts may indicate weak interaction or secondary coordination effects. More informative changes are observed in the C–H and CH_2 stretching regions. The Ni complex shows multiple bands (3230.43, 3174.35 cm^{-1} for C–H; 2963.86, 2903.08 cm^{-1} for CH_2), whereas the Zn complex presents fewer and slightly shifted peaks (e.g., 3172.05 cm^{-1} for C–H and 2981.98 cm^{-1} for CH_2). These variations reflect differences in the ligand environment and suggest that the Ni complex induces greater vibrational splitting, consistent with stronger metal–ligand interactions and structural distortion.

A key diagnostic feature is the C=O stretching vibration. In the Ni complex, this appears at 1786.04 cm^{-1}, which is characteristic of a coordinated carbonyl group and indicates a shift from the free ligand position due to electron donation to the metal center. In contrast, the Zn complex shows an anomalous assignment at 2981.98 cm^{-1}, which is unusually high for a carbonyl stretch and may indicate either misassignment or significant alteration of the vibrational environment; typically, coordination to Zn(II) results in less pronounced shifts compared to Ni(II), consistent with weaker interaction observed in the geometry optimization and FMO results. The CH_3 asymmetric stretching bands are observed in both complexes with comparable values (Ni: 3158.88, 3144.02 cm^{-1}; Zn: 3171.07, 3142.24 cm^{-1}), indicating that methyl groups are not directly involved in coordination but are influenced by the overall electronic environment. Notably, the absence of a Cl–H band in the Ni complex and its reported presence in the Zn complex (2981.98 cm^{-1}) may suggest differences in hydrogen bonding or protonation states, though this assignment should be interpreted cautiously.

The FTIR data support the conclusion that coordination occurs primarily through heteroatoms such as oxygen and nitrogen, with the Ni complex exhibiting stronger interaction as evidenced by more pronounced shifts and band splitting. The Zn complex, on the other hand, shows comparatively smaller perturbations, indicating weaker coordination and

greater retention of the ligand's original vibrational characteristics.

Table 6: FTIR Vibrational Frequencies (Cm^{-1}) Of Functional Groups In Ni(II) And Zn(II) Complexes Indicating Coordination Behavior And Bonding Interactions

Compound	Ni Ligand	Zn Ligand
O-H_{Symm}	3831.30	3837.23
N-H_{Symm}	3599.47, 3595.63	3597.52, 3597.52
C-H_{Symm}	3230.43, 3174.35	3172.05
CH_{2Symm}	2963.86, 2903.08,	2981.98,
CH_{2Assym}	3117.13, 3111.44, 3076.82	3123.83
C=O_{Symm}	1786.04	2981.98
CH_{3Assym}	3158.88, 3144.02	3171.07, 3142.24
Cl-H	-	2981.98

Natural Bond Orbital (NBO) Analysis

The Natural Bond Orbital (NBO) analysis provides a close examination of the donor-acceptor interactions and intramolecular charge transfer in the Ni (II) and Zn (II) mixed-ligand complex in addition to the trends in the geometry optimization and FMO results. Table 7 shows the strongest stabilization interaction between the lone pair of chlorine, n (4) Cl_{33}, and the antibonding orbital of the metal, n (5) Ni_{32}) which has a very high stabilization energy, $E^{(2)}$ of 102.49 kcal/mol. This implies a very high level of donor- acceptor interaction and charge transfer of the ligand to the Ni center and this is a confirmation of strong metal-ligand coordination (Bader et al., 1983). Additional strong interactions include n(1) $N_{26} \rightarrow$ n*(7) Ni_{32} (42.86 kcal/mol) and $\sigma(C_{35}–H_{47}) \rightarrow \sigma^*(Ni_{32}–O_{46})$ (43.03 kcal/mol), further supporting significant electron delocalization involving the metal center. The presence of interactions such as n(2) $N_{40} \rightarrow \pi^*(C_{36}–C_{37})$ (35.17 kcal/mol) and n(3) F43 $\rightarrow \pi^*(C_{36}–C_{37})$ (19.19 kcal/mol) reflects extensive conjugation within the ligand framework. Moreover, interactions involving oxygen and nitrogen donors, such as n(1) $N_{42} \rightarrow \pi^*(C_{34}–O_{41})$ and n(2) $O_{41} \rightarrow \sigma^*(C_{34}–N_{42})$, indicate strong intraligand charge delocalization, which contributes to the overall stability and electronic flexibility of the complex. The relatively high F(i,j) values (up to 0.195) further confirm efficient orbital overlap and strong electronic coupling.

In contrast, the Zn complex shows generally lower stabilization energies, indicating weaker donor–acceptor interactions. The interactions include n(1) $N_{38} \rightarrow \pi^*(C_{33}–O_{40})$ (25.88 kcal/mol) and n(2) $O_{40} \rightarrow \sigma^*(C_{33}–N_{38})$ (24.10 kcal/mol), which are primarily intraligand in nature. Metal-involved interactions such as n(1) $N_{37} \rightarrow \sigma^*(Zn_{27}–Cl_{29})$ (19.47 kcal/mol) and n(1) $O_{30} \rightarrow \sigma^*(Zn_{27}–O_{30})$ (13.53 kcal/mol) are comparatively weaker than those observed in the Ni complex, reflecting reduced metal–ligand covalency. Additionally, the back-donation interaction $\sigma(Zn_{27}–O_{30}) \rightarrow$ n(2) N_{37} (11.45 kcal/mol) is relatively small, suggesting limited electron density redistribution involving the Zn center. The lower F(i,j) values overall also point to weaker orbital overlap and less efficient charge transfer.

The results of NBO have clearly revealed that the Ni complex is dominated by strong metal-centered donor-acceptor interaction, high level of charge delocalization and high stabilization energy, which is a characteristic of a system that is more covalent and electronically interacting. Conversely, the interactions between the Zn complex and the other elements are more localized with a lower stabilization energy, in line with a more ionic nature of the bonding and less electronic delocalization.

Table 7: Natural Bond Orbital (NBO) Analysis Showing Donor–Acceptor Interactions, Stabilization Energies $E^{(2)}$, Energy Differences, And Fock Matrix Elements for Ni and Zn Complexes

Compound	Donor (i)	Acceptor (j)	$E^{(2)}$ kcal/mol	E(j) – E(j)	F(i,j)
Ni Ligand	n (4) Cl_{33}	n*(5) Ni_{32}	102.49	0.46	0.195
	n (3) F_{43}	π^* C_{36} - C_{37}	19.19	0.41	0.083
	n (1) N_{42}	π^* C_{34} - O_{41}	9.11	0.29	0.049
	n (2) O_{41}	σ^* C_{34} - N_{42}	15.29	0.51	0.079
	n (2) N_{40}	π^* C_{36} - C_{37}	35.17	0.19	0.081
	σ C_{35} - H_{47}	σ^* Ni_{32} - O_{46}	43.03	0.40	0.126
	n (1) N_{26}	n*(7) Ni_{32}	42.86	0.76	0.165
Zn Ligand	n (2) O_{40}	σ^* C_{33} - N_{38}	24.10	0.56	0.105
	n (3) F_{39}	π^* C_{31} - C_{32}	19.59	0.41	0.084
	n (1) N_{38}	π^* C_{33} - O_{40}	25.88	0.31	0.082
	n (1) N_{37}	σ^* Zn_{27} -Cl_{29}	19.47	0.68	0.106
	n (1) O_{30}	σ^* Zn_{27} - O_{30}	13.53	0.88	0.100
	σ Zn_{27} - O_{30}	n (2) N_{37}	11.45	0.10	0.045

Molecular Electrostatic Potential (MESP) Analysis

The Molecular Electrostatic Potential (MESP) analysis of the Ni(II) and Zn(II) mixed-ligand complexes provides a visual and quantitative understanding of charge distribution, reactive sites, and potential intermolecular interaction behavior. From Figure 13, regions of negative electrostatic potential (typically shown in red/yellow) correspond to electron-rich areas prone to electrophilic attack, while positive regions (blue) indicate electron-deficient sites favorable for nucleophilic interactions **(**Parr et al., 1988). In the Ni complex, the MESP surface

shows a relatively extended distribution of electron density across the ligand framework, with pronounced negative potential localized around electronegative atoms such as oxygen, nitrogen, and halogen substituents. These regions appear more continuous and delocalized, indicating effective charge dispersion throughout the molecule. The positive regions are less localized and moderately distributed around hydrogen atoms and parts of the metal coordination sphere. This pattern reflects strong metal–ligand interaction and significant electron delocalization, consistent with the small HOMO–LUMO gap and high softness observed earlier. The broader spread of electron density suggests that the Ni complex has multiple potential reactive sites, enhancing its ability to participate in intermolecular interactions such as hydrogen bonding or coordination with biological targets. In contrast, the Zn complex exhibits a more localized and segmented electrostatic potential distribution. The negative regions are still concentrated around heteroatoms (O, N, and F), but they appear more confined and less delocalized compared to the Ni complex. Additionally, a more distinct positive region is observed around the Zn center and adjacent coordination sites, indicating a relatively higher electron deficiency at the metal core. This localization aligns with the larger HOMO–LUMO gap and higher hardness, suggesting reduced polarizability and a more stable electronic structure. The separation between electron-rich and electron-poor regions implies more defined reactive sites but lower overall reactivity compared to the Ni complex.

MESP analysis confirms that the Ni complex possesses a more delocalized charge distribution and enhanced electronic flexibility, which can facilitate stronger and more diverse interactions with surrounding molecules. On the other hand, the Zn complex displays a more localized electrostatic profile with clearer differentiation between nucleophilic and electrophilic regions, indicative of greater stability and more selective interaction behavior.

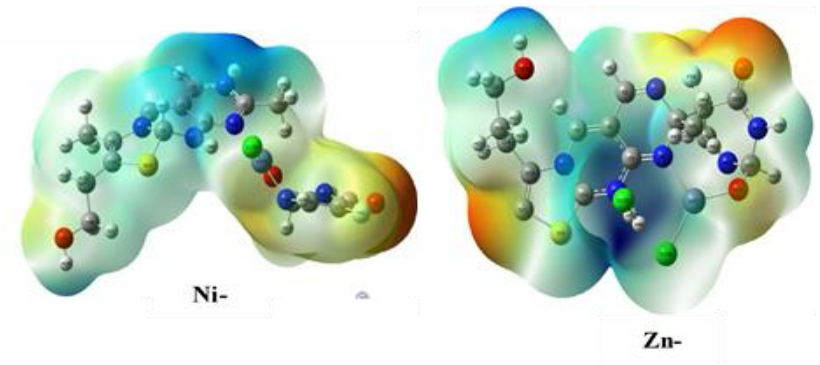

Figure 13: Molecular Electrostatic Potential (MESP) Surfaces of Ni (II) and Zn (II) Complexes Highlighting Regions of Electrophilic and Nucleophilic Reactivity

Quantum Theory of Atoms in Molecules (QTAIM)

The Quantum Theory of Atoms in Molecules (QTAIM) analysis, supported by the molecular image in Figure 14, provides a rigorous description of bonding interactions, electron density distribution, and the nature of intra- and intermolecular contacts in the Ni(II) and Zn(II) complexes.

In the Ni–ligand system, the presence of bond critical points (BCPs) such as Ni_{32}–N_{26}, Cl_{33}–H_{44}, and O_{46}–H_{30} confirms the existence of both coordination bonds and secondary interactions like hydrogen bonding. The electron density values ρ(r) at these BCPs are moderate (e.g., 0.0815 for Ni–N and 0.420 for Cl–H), while the Laplacian values $\nabla^2\rho(r)$ indicate closed-shell interactions typical of coordination bonds and hydrogen bonds rather than purely covalent bonds (T.Schaafsma, 1965). Importantly, the energy density ratio |V(r)|/G(r) for Ni–N (≈1.05) and Cl–H (≈1.14) lies close to unity, suggesting partially covalent character with some degree of electron sharing as shown on Table 8. This is consistent with earlier NBO and FMO results indicating significant metal–ligand orbital overlap. The ELF values are relatively low to moderate, further supporting delocalized electron density rather than strong localization. Additionally, the ellipticity (ε) values are generally small (e.g., 5.50×10^{-2} for Ni–N), indicating stable bonding with limited π-character distortion. The molecular graph in the image visually supports these findings by showing well-defined bond paths between Ni and donor atoms, along with multiple weak intermolecular interactions (depicted as dotted lines), reflecting a highly interconnected and electronically delocalized system.

In contrast, the Zn–ligand complex exhibits BCPs such as Zn_{27}–Cl_{28}, Cl_{29}–N_9, and H_{16}–O_{25}, highlighting both coordination and weak noncovalent interactions. The electron density at Zn–Cl (ρ(r) = 0.0742) is comparable to Ni–N but is accompanied by a higher Laplacian ($\nabla^2\rho(r)$ = 0.241), indicating a more pronounced closed-shell, ionic interaction. The |V(r)|/G(r) ratio for Zn–Cl (≈1.20) suggests a slightly stronger interaction than purely electrostatic, but still less covalent than typical shared interactions. Notably, some interactions, such as Cl_{29}–N_9, show |V(r)|/G(r) < 1 (≈0.839), indicating predominantly electrostatic or van der Waals character. The relatively low ρ(r) values for interactions like Cl–H (0.00422) further confirm weak hydrogen bonding. ELF values remain low, reflecting limited electron localization, while the ellipticity for certain interactions (e.g., Cl_{29}–N_9 with ε ≈ 12.3) is unusually high, suggesting significant anisotropy or instability in electron distribution, possibly due to weak or strained interactions.

Comparatively, the QTAIM results clearly show that the Ni complex has stronger and more balanced metal–ligand interactions with partial covalent character, supported by moderate electron density, |V(r)|/G(r) ratios near unity, and stable ellipticity values. The Zn complex, on the other hand, is dominated by more ionic and weaker interactions, with lower electron densities and greater variability in bonding characteristics. Figure 14 further reinforces this interpretation: the Ni complex displays a denser network of bond paths and interactions, while the Zn complex shows more localized and fewer strong connections. QTAIM analysis confirms that the Ni complex is electronically more integrated and exhibits stronger coordination with partial covalency, whereas the Zn complex is characterized by weaker, more electrostatic interactions.

Table 8: QTAIM Topological Parameters At Bond Critical Points (Bcps), Including Electron Density P(R), Laplacian ∇²P(R), Kinetic Energy Density G(R), Potential Energy Density V(R), Energy Density Ratio |V(R)|/G(R), Electron Localization Function (ELF), And Ellipticity (E) For Ni And Zn Complexes.

Compounds	BCPs	Connected Atoms	ρ(r)	∇^2 ρ(r)	G(r)	V(r)	|V(r)|/G(r)	ELF	ε
Ni-Ligand	62	Cl_{33}-H_{44}	4.20E-01	8.70E-01	2.51E-01	-2.85E-01	1.14E+00	2.51E-01	1.67E-02
	64	H_{18}-H_{14}	8.35E-03	3.58E-02	6.97E-03	-5.00E-03	7.17E-01	1.96E-02	1.19E+00
	88	Ni_{32}-N_{26}	8.15E-02	4.92E-01	1.28E-01	-1.34E-01	1.05E+00	1.05E-01	5.50E-02
	98	O_{46}-H_{30}	2.78E-02	9.70E-02	2.28E-02	-2.14E-02	9.39E-01	9.35E-02	1.17E-01
Zn-Ligand	50	Cl_{28}-H_{45}	2.63E-02	5.81E-02	1.54E-02	-1.63E-02	1.06E+00	1.58E-01	5.53E-02
	51	Cl_{28}-Zn_{27}	7.42E-02	2.41E-01	7.58E-02	-9.12E-02	1.20E+00	1.97E-01	2.92E-02
	60	Cl_{29}-N_{9}	7.78E-02	2.45E-02	5.27E-03	4.42E-03	8.39E-01	2.68E-02	12.3E+00
	63	Cl_{29}-H_{42}	4.22E-03	1.43E-02	2.88E-03	2.19E-03	7.60E-01	1.19E-02	1.20E-01
	105	H_{16}-O_{25}	1.75E-02	5.45E-02	1.29E-02	-1.21E-02	9.38E-01	6.48E-02	8.28E-02

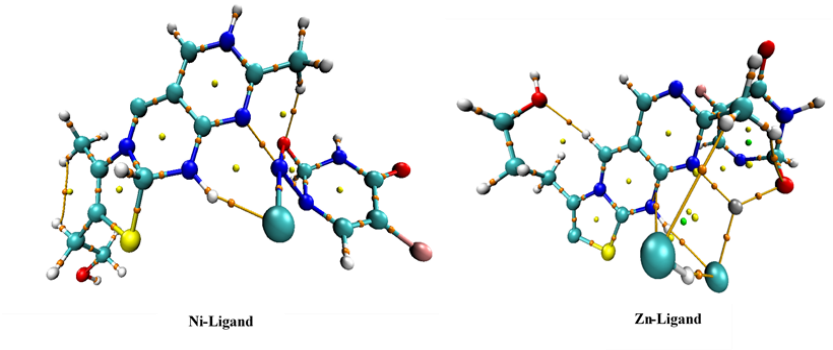

Figure 14: QTAIM Molecular Graphs of Ni (II) and Zn (II) Complexes Showing Bond Critical Points and Bond Paths

Non-Covalent Interactions

The non-covalent interaction (NCI) analysis of the Ni–ligand and Zn–ligand complexes provides detailed insight into the nature and spatial distribution of weak interactions that contribute to their structural stability. The reduced density gradient (RDG) isosurfaces are color-mapped according to the sign of the eigenvalue (λ_2) of the electron density Hessian, enabling clear identification of interaction types: blue regions indicate strong attractive interactions, green regions correspond to weak van der Waals (vdW) forces, and red regions represent steric repulsion **(**Lefebvre et al., 2017) From **Figure 15,** the Ni–ligand complex, prominent blue isosurfaces are observed around the metal–ligand coordination sites, confirming strong attractive interactions between the Ni center and donor atoms such as nitrogen or oxygen. Additionally, widespread green regions across the ligand framework suggest significant vdW stabilization, while localized red patches near crowded coordination environments indicate steric repulsion arising from ligand packing. In comparison, the Zn–ligand complex exhibits similar but more diffuse blue regions at coordination sites, consistent with the relatively more ionic and less covalent nature of Zn–ligand bonding. The green vdW isosurfaces are more broadly distributed, suggesting enhanced structural flexibility, and the reduced presence of red regions indicates lower steric congestion around the Zn-center.

NCI analysis reveals that both complexes are stabilized by a combination of coordination interactions and vdW forces, with the Ni–ligand system displaying stronger and more localized attractive interactions leading to a more rigid structure, while the Zn–ligand system exhibits comparatively weaker, more delocalized interactions associated with greater flexibility.

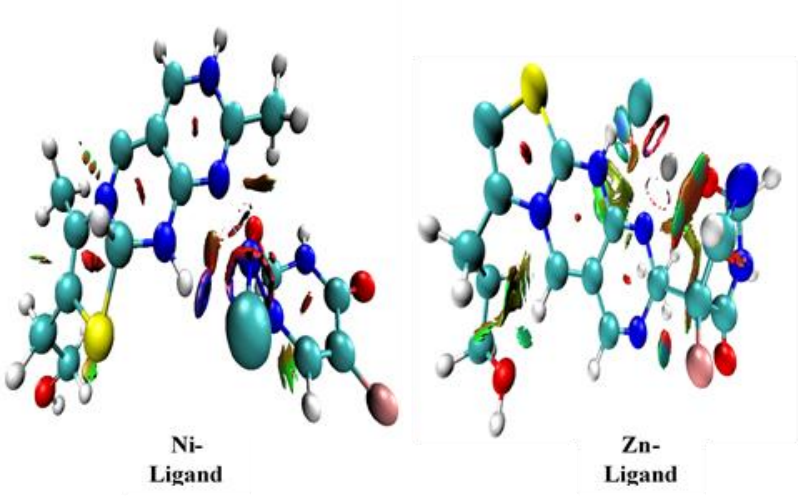

Figure 15: Non-Covalent Interaction (NCI) RDG Is Surfaces for Ni (II) and Zn (II) Complexes, Colour according To Sign (λ_2) ρ, Indicating Attractive, Van Der Waals, And Steric Interactions

MOLECULAR DOCKING

Protein Validation

The ATP-binding domain of *Escherichia coli* DNA gyrase subunit B is represented by PDB ID: 1KZN **(**Lafitte et al., 2002). DNA gyrase is a well-known target for the development of antibacterial drugs because it is an essential bacterial type II topoisomerase that introduces negative supercoils into DNA during transcription and replication. The ATP-binding pocket, a recognised interaction location for several antibacterial drugs, including Ciprofloxacin, whose inhibition stops ATP hydrolysis and stops bacterial cell multiplication, is why the GyrB subunit was chosen. Because of its stable conformation, well-defined active site, cavity detection, and interaction analysis, the 1KZN structure was selected. Moreso, Lanosterol 14-alpha demethylase from Candida albicans is associated with PDB ID: 5TZ1 **(**Hargrove et al., 2017). This enzyme, often referred to as CYP51, is one of the most significant molecular targets for the development of antifungal medications and is crucial to the manufacture of ergosterol, a necessary component of the fungal cell membrane. Fungal growth is inhibited, and membrane integrity is lost when this enzyme is inhibited because ergosterol synthesis is disrupted. The 5TZ1 structure was chosen because of its well-defined active site with a bound azole inhibitor, stable conformation, and good resolution.

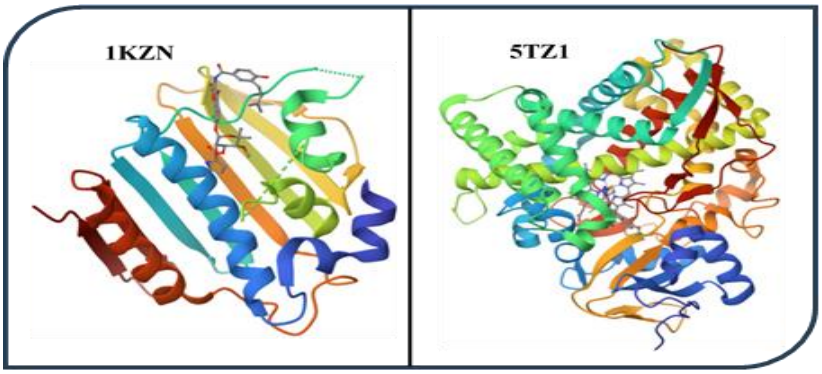

Figure 16: Structures of the Target Proteins (1KZN and 5TZ1) Downloaded from the Protein Data Bank

Molecular Docking Result

The complexes (Ni-Ligand and Zn-Ligand), the selected standard antibacterial drug Ciprofloxacin (CIPRO), and the antifungal drug Fluconazole (FLUCO) were docked against the selected ligands (1KZN and 5TZ1); the results of this interaction along with the docking coordinates for the proteins are presented in **Table 9**. To begin with, Ni-Ligand interacted with 1KZN and recorded a Moldock score of -153.39 kcal/mol and a Rerank (-101.75 kcal/mol) indicating a high affinity, supported by three conventional hydrogen bonds (Val 71, THR 65, and Asn 46) and various steric interactions to infer stronger binding orientation **(**Wishart et al., 2018). Consequently, Ni-Ligand exhibited a binding affinity of -134.94 kcal/mol supported by a H-bond (-4.70) and a robust presence of residues from steric interactions and significant hydrogen bond, active around the OH and NH_2 species of the ligand, generating important residues (Ser, Val, and Asn), exhibiting strong binding potential. Afterwards, the selected antibacterial standard drug (CIPRO) was docked with the same target protein, generating a comparatively lesser binding score of -117.39 kcal/mol, along with two hydrogen bonds (Arg 136 and Gly 77). Comparatively, the test compounds have depicted outstanding inhibitory potential to serve as a potential antibacterial drug, having demonstrated higher binding potentials and registered a greater number of hydrogen bonds in their interactions to outperform CIPRO which had lesser binding affinity and fewer number of hydrogen bonds.

On the other hand, the test compounds were docked with the fungal target protein ID: 5TZ1; as shown in Table 1, Ni-Ligand generated a binding affinity of -129.48 kcal/mol, followed by a Rerank score of -100.21 kcal/mol with significant hydrogen interaction (Ser 63) at the OH-specie of the ligand, along with some steric interaction to support the

docking conformation. Moving further, Zn-Ligand recorded a more impressive profile with a binding affinity of -131.12 kcal/mol with a significant H-bond value (-2.11) and favourable residues (Ile 471, Tyr 132, and Arg 381), indicative of strong docking conformation support. The docking profile exhibited by the test compounds were juxtaposed by the standard drug-FLUCO; here, FLUCO exhibited a high positive Moldock score (883.83 kcal/mol) probably due to steric clashes; however, the Rerank score (-71.37 kcal/mol) which serve as a more refined score was used to compare the reports; moreover, the interaction exhibited a hydrogen bond Gln 67. Comparatively, the interactions showed outstanding performance in inhibiting the target with a favourable profile over the standard drug to serve as potent antifungal drug agents. The simulated outcome of the test compounds has distinctly shown outstanding performances in binding with the target proteins, exhibiting promising potential that should be further explored for their therapeutic potentials.

Table 9: The Molecular Docking Result, Showing the Moldock Scores, the Rerank, Hydrogen Bond, and the Corresponding H-Bond Distances

Interaction	Moldock Score (kcal/mol)	Rerank (kcal/mol)	H-Bond	Hydrogen-bond
Ni-Ligand/1KZN	-153.39	-101.75	-6.47	Val 71, Thr 65, Asn 46
Zn-Ligand/1KZN	-134.92	-21.19	-4.70	Ser 121, Val 120, Asn 46
CIPRO/1KZN	-117.39	-75.21	-3.01	Arg 136, Gly 77
Ni-Ligand/5TZ1	-129.48	-100.21	-2.90	Ser 63
Zn-Ligand/5TZ1	-131.12	-97.32	-2.11	Ile 471, Arg 381, Tyr 132
FLUCO/5TZ1	883.83	-71.37	-4.11	Gln 67
Protein Coordinates				
Protein ID: 1KZN	X: 22.11, Y: 19.59, Z: 41.60, RADIUS: 15			
Protein ID: 5TZ1	X: 57.23, Y: 51.35, Z: 20.63, RADIUS: 38			

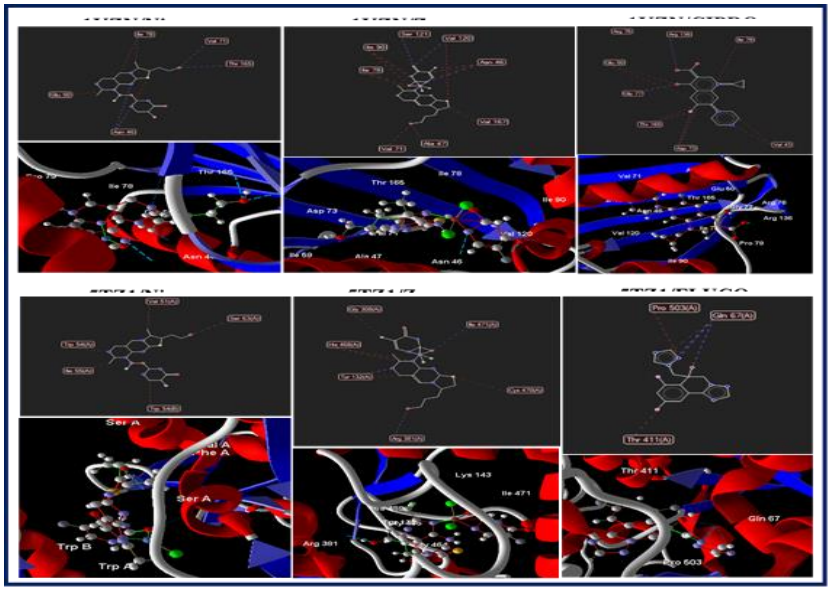

Figure 17: Showing the 2D and 3D Visualization for the Interaction of the Test Complexes and the Standard Drugs against the Target Proteins 1KZN and 5TZ1

CONCLUSION

This study comprehensively explored the structural, electronic, and biological properties of Ni(II) and Zn(II) mixed-ligand complexes of 5-fluorouracil–thiamine HCl using integrated computational approaches. Spectroscopic analysis indicated that the 5-flourouracil acts as a bidentate ligand while thiamine HCl acts a monodentate ligand in the formation of the complexes. Both compounds exhibit good biological activity as antibacterial, antifungal and antioxidant agents. Geometry optimization demonstrated that the Ni(II) complex exhibits shorter and stronger metal–ligand bonds, particularly with nitrogen and oxygen donor atoms, reflecting enhanced covalent character and greater structural distortion compared to the Zn(II) complex, which showed relatively longer and more ionic interactions. Frontier molecular orbital (FMO) analysis revealed that the Ni complex possesses a significantly smaller HOMO–LUMO energy gap, lower global hardness, and higher softness, indicating higher chemical reactivity and enhanced electron delocalization, whereas the Zn complex exhibited a larger band gap and greater stability.

The NBO results confirmed stronger donor–acceptor interactions and higher stabilization energies in the Ni complex, particularly involving metal-centered orbitals, while the Zn complex displayed weaker and more localized interactions. QTAIM analysis indicated partial covalent character in Ni–ligand bonding with stronger electron density at bond critical points, whereas the Zn complex was dominated by closed-shell, electrostatic interactions. Additionally, NCI analysis demonstrated that the Ni complex is stabilized by stronger and more localized attractive interactions, resulting in a more rigid structure, while the Zn

complex exhibits more diffuse van der Waals interactions, contributing to greater flexibility.

Importantly, molecular docking studies provided strong biological validation of these computational findings. The test complexes showed superior binding affinities against both bacterial (1KZN) and fungal (5TZ1) target proteins compared to standard drugs. Ni-Ligand exhibited excellent antibacterial activity with a Moldock score of −153.39 kcal/mol and strong hydrogen bonding interactions (Val 71, Thr 65, and Asn 46), outperforming the standard drug Ciprofloxacin, which showed a lower binding affinity (−117.39 kcal/mol) and fewer hydrogen bonds. Similarly, both complexes demonstrated remarkable antifungal activity, with Zn-Ligand showing particularly strong binding (−131.12 kcal/mol) and favorable interactions with key residues (Ile 471, Tyr 132, and Arg 381), surpassing the performance of Fluconazole, which exhibited weaker interaction profiles.

Combined computational and docking results clearly establish that the Ni (II) complex is more reactive, electronically delocalized, and biologically active due to stronger metal–ligand covalency and enhanced intermolecular interactions. The Zn (II) complex, while comparatively less reactive, offers greater stability and controlled interaction behavior. The superior docking performance of the complexes relative to standard drugs highlights their potential as promising antibacterial and antifungal agents, warranting further experimental and pharmacological investigation.

REFERENCES

Ahmed, Y. M., Ashmawy, A. M., Abbas, A. A., & Mohamed, G. G. (2023). Synthesis, characterization, antibacterial, antioxidant activities, density functional theory, and molecular docking studies of new organic metal complexes and links to application of corrosion inhibitors. *Applied Organometallic Chemistry*, *37*(4), e7015.

Aihara, J. I. (1999). Reduced HOMO− LUMO gap as an index of kinetic stability for polycyclic aromatic hydrocarbons. *The Journal of Physical Chemistry A*, *103*(37), 7487-7495.

AL-Nama, K. S., Saeed, I. A., & Mohammed, A. F. (2025). Synthesis, characterization, DFT, molecular docking, and in vitro screening of metal chelates incorporating Schiff base. *Bulletin of the Chemical Society of Ethiopia*, *39*(4), 687-701.

Althubeiti, K. (2025). Synthesis and characterization of the Co (ii), Ni (ii), and Cu (ii) complexes with a 1, 2, 4-triazine derivative ligand. *Open Chemistry*, *23*(1), 20250186.

Berman, H. M., Westbrook, J., Feng, Z., Gilliland, G., Bhat, T. N., Weissig, H., & Bourne, P. E. (2000). The protein data bank. *Nucleic acids research*, *28*(1), 235-242.

Bitencourt-Ferreira, G., & de Azevedo Jr, W. F. (2019). Molegro virtual docker for docking. In *docking screens for drug discovery* (pp. 149-167). New York, NY: Springer New York.

Bader, R. F. W., Slee, T. S., Cremer, D., & Kraka, E. (1983). Description of conjugation and hyperconjugation in terms of electron distributions. *Journal of the American Chemical Society*, *105*(15), 5061-5068.

Carballo Rial, R., Castiñeiras Campos, A., Domínguez Martín, A., García Santos, I., & Niclós Gutiérrez, J. (2012). Solid state structures of cadmium complexes with relevance for biological systems.

Elgazar, S. M., Abd El-Karim, A. T., Mahmoud, W. H., & El-Sherif, A. A. (2025). Comprehensive analysis of nitrogen–oxygen schiff base derived from Triazole and its metal complex: synthesis, structural characterization, and biological activities with theoretical insights for anti-helicobacter pylori, antitumor, and anti-covid-19 applications. *Egyptian Journal of Chemistry*, *68*(3), 169-191.

Glendening, E. D., Landis, C. R., & Weinhold, F. (2019). NBO 7.0: New vistas in localized and delocalized chemical bonding theory. *Journal of computational chemistry*, *40*(25), 2234-2241.

Gmeiner, W. H., & Okechukwu, C. C. (2023). Review of 5-FU resistance mechanisms in colorectal cancer: Clinical significance of attenuated on-target effects. *Cancer Drug Resistance, 6*(2), 257–272. https://doi.org/10.20517/cdr.2022.136.

Hargrove, T. Y., Friggeri, L., Wawrzak, Z., Qi, A., Hoekstra, W. J., Schotzinger, R. J., ... & Lepesheva, G. I. (2017). Structural analyses of Candida albicans sterol 14α-demethylase complexed with azole drugs address the molecular basis of azole-mediated inhibition of fungal sterol biosynthesis. *Journal of Biological Chemistry*, *292*(16), 6728-6743.

Hellweg, A., & Rappoport, D. (2015). Development of new auxiliary basis functions of the Karlsruhe segmented contracted basis sets including diffuse basis functions (def2-SVPD, def2-TZVPPD, and def2-QVPPD) for RI-MP2 and RI-CC calculations. *Physical Chemistry Chemical Physics*, *17*(2), 1010-1017.

Hemingway, T. (2020). *Chemistry of a Biscarborane Dithiol and Its Nickel (II) Complex* (Doctoral dissertation, University of South Carolina).

Hrubša, M., Siatka, T., Nejmanová, I., Vopršalová, M., Kujovská Krčmová, L., Matoušová, K., & Oemonom. (2022). Biological properties of vitamins of the B-complex, part 1: vitamins B1, B2, B3, and B5. *Nutrients*, *14*(3), 484.

Inah, B. E., Azogor, N. F., Akpan, H. T., Levi, O. E., Charlie, D., & Adeleye, A. P. (2025). Exploring the adsorption properties of PTFE-decorated and metal doped covalent organic frameworks for environmental cleanup: a computational outlook. *Computational and Theoretical Chemistry*, *1248*, 115202.

Jamil, Y., Al-Baseer, M. M., Al-Akhali, B., & Alhakimi, A. N. (2025). Synthesis and characterization of mixed ligand complexes of Fluconazole drug and glycine with some transition metals: antifungal study. *Sana'a University Journal of Applied Sciences and Technology*, *3*(2), 718-729.

Koller, D., Blaha, P., & Tran, F. (2013). Hybrid functionals for solids with an optimized Hartree–Fock mixing parameter. *Journal of Physics: Condensed Matter*, *25*(43), 435503.

Lafitte, D., Lamour, V., Tsvetkov, P. O., Makarov, A. A., Klich, M., Deprez, P., & Gilli, R. (2002). DNA gyrase interaction with coumarin-based inhibitors: the role of the

hydroxybenzoate isopentenyl moiety and the 5 '-methyl group of the noviose. *Biochemistry*, *41*(23), 7217-7223.

Lefebvre, C., Rubez, G., Khartabil, H., Boisson, J. C., Contreras-García, J., & Hénon, E. (2017). Accurately extracting the signature of intermolecular interactions present in the NCI plot of the reduced density gradient versus electron density. *Physical Chemistry Chemical Physics*, *19*(27), 17928-17936. Accessed: Dec. 20, 2025. [Online]. Available: https://pubs.rsc.org/en/content/articlehtml/2005/zq/c7cp02110k

Liu, C. (2022). Anion induced synthesis and crystal structures of Schiff base copper (II) and zinc (II) complexes with antibacterial activity. *Russian Journal of Coordination Chemistry*, *48*(6), 385-396.

Marinova, P. E., & Blazheva, D. E. (2025). A Comprehensive Review of the Synthesis, Characterization, and Therapeutic Potential of Gold, Platinum, and Ruthenium Complexes and Organic Compounds.

Melo-Betances, E., Rodríguez-Bautista, C. C., & Núñez-Sellés, A. J. (2025). Synthesis of mangiferin derivatives, complexes, and carriers as potential therapeutic candidates for cancer treatment: An update. *Frontiers in pharmacology*, *16*, 1598719.

Omer, P. K., Aziz, N. M., & Omer, R. A. (2024). Comprehensive review of metal-based coordination compounds in cancer therapy: from design to biochemical reactivity. *Reviews in Inorganic Chemistry*, *44*(4), 699-710.

Parr, R. G., Szentpály, L. V., & Liu, S. (1999). Electrophilicity index. *Journal of the American Chemical Society*, *121*(9), 1922-1924.

Pasieczna-Patkowska, S., Cichy, M., & Flieger, J. (2025). Application of Fourier transform infrared (FTIR) spectroscopy in characterization of green synthesized nanoparticles. *Molecules*, *30*(3), 684.

She, W. J., Cui, Y. F., Liu, C., and Wang, L. (2020). Structurally characterized dinuclear zinc (II) and copper (II) coumarin-based N2O2-donor complexes: syntheses, Hirshfeld analyses and fluorescent properties. *Transition Metal Chemistry*, *45*(5), 363-372.

Silva, V. R., Corrêa, R. S., Santos, L. D. S., Soares, M. B. P., Batista, A. A., and Bezerra, D. P. (2018). A ruthenium-based 5-fluorouracil complex with enhanced cytotoxicity and apoptosis induction action in HCT116 cells. *Scientific reports*, *8*(1), 1-13.

T. Schaafsma, J. K.-T. J. of C. Physics, and undefined 1965, "Electron Delocalization and Charge Transfer," *pubs.aip.org*, Accessed: Jan. 22, 2026. [Online]. Available: https://pubs.aip.org/aip/jcp/article-abstract/42/1/438/81386.

Tyagi, A., Banerjee, S., Cherusseri, J., & Kar, K. K. (2020). Characteristics of transition metal oxides. In *Handbook of Nanocomposite Supercapacitor Materials I: Characteristics* (pp. 91-123). Cham: Springer International Publishing.

Wishart, D. S., Feunang, Y. D., Guo, A. C., Lo, E. J., Marcu, A., Grant, J. R., ... & Wilson, M. (2018). DrugBank 5.0: a major update to the DrugBank database for 2018. *Nucleic acids research*, *46*(D1), D1074-D1082.

Yadav, M., Yadav, D., Singh, D. P., & Kapoor, J. K. (2025). Macrocyclic Schiff base complexes of Zn (II), Cu (II), Co (II), and Ni (II) targeting topoisomerase IIβ: Synthesis, docking, and evaluation as potential anticancer agents. *Applied Organometallic Chemistry*, *39*(3), e7885.

Yusuff, O. K., Abdul Raheem, M. A. O., Mukadam, A. A., and Sulaimon, R. O. (2019). Kinetics and Mechanism of the Antioxidant Activities of C. olitorius and V. amygdalina by Spectrophotometric and DFT Methods. *ACS omega*, *4*(9), 13671-13680.